Nanoscale

Accepted Manuscript

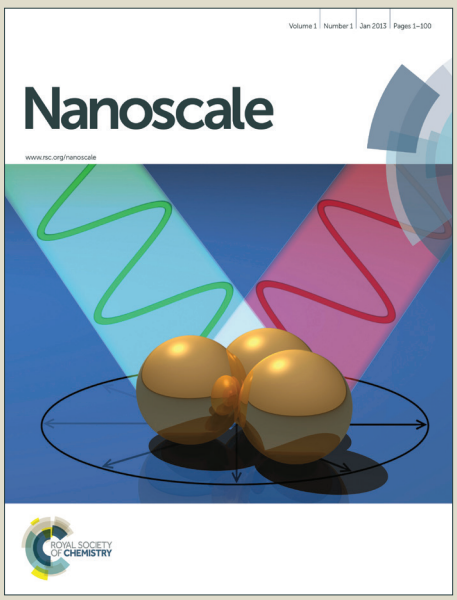

ROYAL SOCIETY OF CHEMISTRY

www.rsc.org/nanoscale

Nanoscale

RSCPublishing

COMMUNICATION

300 mm Wafer-Level, Ultra-Dense Arrays of Au-Capped Nanopillars with sub-10 nm Gaps as Reliable SERS Substrates

Cite this: DOI: 10.1039/x0xx00000x

Received 19th July 2014,
Accepted 00th January 2014

DOI: 10.1039/x0xx00000x

www.rsc.org/

Jiaqi Li*[ab], Chang Chen*[ab], Hilde Jans[a], Xiumei Xu[a], Niels Verellen[ab], Ingrid Vos[a], Yasuaki Okumura[ac], Victor V. Moshchalkov[b], Liesbet Lagae[ab] and Pol Van Dorpe[ab]

The 193 nm deep UV immersion lithography is leveraged to fabricate highly dense and uniform arrays of Au-capped Si nanopillars on a 300 mm wafer level, and the substrates are applied in Surface Enhanced Raman Spectroscopy for reliable molecule detections. Due to the sub-10 nm gap sizes and ultra-high array density with the lattice constant less than 100 nm, our nanopillar based substrates outperform the current commercial products in terms of the signal intensity, reproducibility and fabrication scale.

Introduction

Surface enhanced Raman spectroscopy (SERS) is a well-known and powerful molecular detection technique which is mainly enabled by the electromagnetic (EM) field enhancement on plasmonic nanostructured surfaces to compensate for the weak scattering cross sections of the target molecules. Extensive research has been carried out in the exploration of SERS substrates with enhanced and uniform signal generations. To obtain largely enhanced SERS intensities, regions of strongly enhanced EM field, referred to as plasmonic hot spots, are carefully engineered. This can be achieved by either adjusting the compositions and geometries of the nanostructures for a better aligned plasmonic resonances with the excitation and Raman scattering wavelengths, [1–3] or concentrating target molecules in gap-dominated small volumes.[4–6] Next to the SERS intensity, the uniformity of the SERS signal across the substrate and the reproducibility among different samples is extremely important. Plasmonic nanostructures formed by self-assembly process can form regular arrays up to the millimeter scale with well controllable spacing and produce excellent signal uniformity.[7–10] The commercially available SERS substrate, Klarite™, consisting of gold layer coated arrays of inverted pyramids etched in silicon, highlights a reproducibility landmark with better than 10% relative standard deviation level.[11,12] Although the reproducibility offered by the Klarite™ substrates is already a big improvement compared to aggregate-type substrates,[7] several applications require even better reproducibility and uniformity. In addition, the increase in reproducibility is typically accompanied by a drop in the SERS enhancement factor. Wafer-scale fabrication of uniform, reproducible and stable SERS substrates with high enhancement factor remains a very critical step in the realization of commercial SERS applications.[13–16]

Nanopillar structures are one of the most promising SERS substrates in the sense that they provide a three-dimensional environment beneficial for molecular accessibility and formation of gap-rich plasmonic nanostructures.[14,15,17] Such substrates have been fabricated by a variety of techniques based on nanoimprint,[14] reactive ion etching,[15,17–19] chemical etching,[20,21] e-beam[17,22,23] and interference lithography,[24,25] as well as by anodic aluminum oxide templates.[3,5] Nevertheless, high density of regularly spaced pillar substrates which is required by good signal reproducibility is still not achievable with most large scale lithography methods. Here we report a SERS substrate that is scalable and inherently uniform with a large enhancement factor. As schematically described in **Figure 1**a, we leverage the state-of-the-art standard CMOS patterning technology on 300 mm wafers by fabricating ultra-dense periodic arrays of silicon nanopillars (Figure 1b and c). By deep ultraviolet (DUV) immersion lithography with sequential double line exposures using a mask of 45 nm width and 45 nm spacing, a pitch down to 90 nm has been accomplished. The plasmonic hot spots are subsequently obtained by coating the nanopatterned silicon substrate with a thin Au film, and by carefully controlling the thickness of the Au film, sub-10 nm gaps are achieved (Figure 1 d and e). To our best knowledge, SERS substrates with such high regular array density and small gap size have not been

reported before. Our substrates highlight not only a superior SERS signal reproducibility, but also easy accessibility to the target analyte and good robustness. We further evaluate the SERS performance under both 633 nm and 785 nm laser illumination, and a simplified finite difference time domain (FDTD) model is adopted to interpret the correlation between the SERS intensity and the Au deposition thickness.

Results and discussions

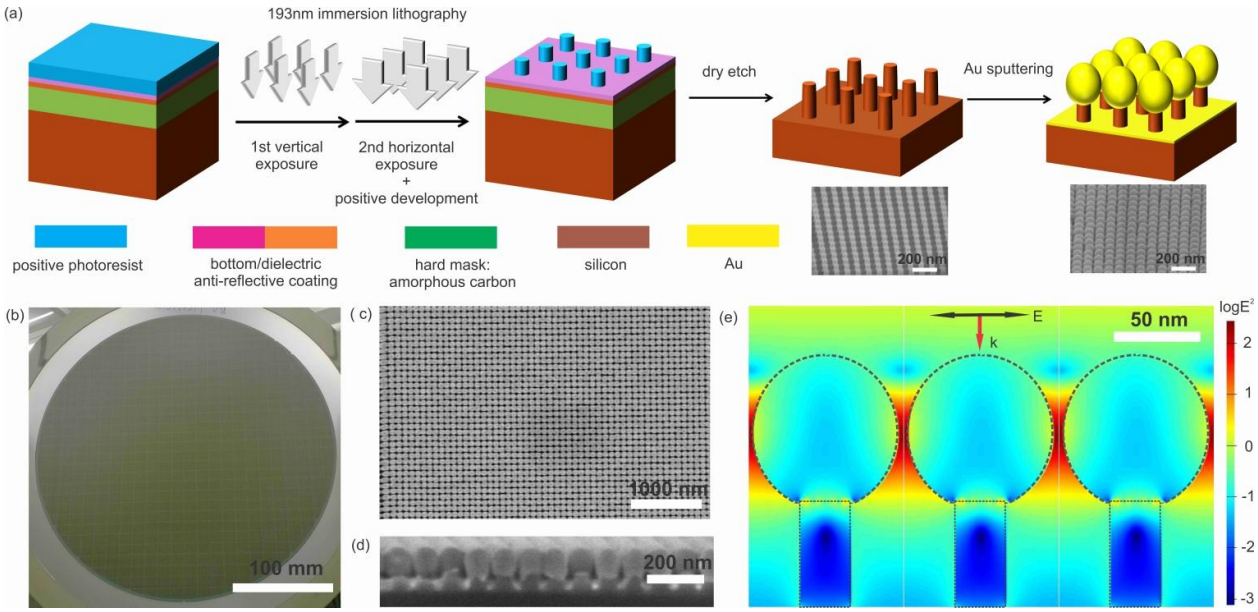

Figure 1. (a) Schematic of the fabrication of Au-capped nanopillar substrates by DUV immersion lithography and Au sputtering. Two SEM images are shown below the corresponding nanostructures. (b) An optical image of the 300 mm wafer Si nanopillar substrate. SEM images of the ultra-dense nanopillar array with 80 nm Au sputtering on 70 nm height Si nanopillars viewed from (c) top, and (d) side cross-section. (e) Corresponding FDTD simulated profile of the electric field enhancement distribution at the 785 nm light excitation. The black dashed lines are the outline of the Au capped Si nanopillars. The black and red arrows indicates the polarization and incidence direction of the excitation light, respectively.

The properties of the nanopillars could be fine-tuned by adjusting the Si etch time and the Au deposition thickness. We investigated relatively short pillars with heights H_{pillar}=70 nm and 150 nm to ensure good robustness for the successive fabrication steps and measurements. Detailed fabrication and characterization methods are available in Section 1 of the supporting information. It is generally accepted that the SERS enhancement is optimal between nanogaps. Therefore, on the Si nanopillars with the diameter of 30 nm we sputtered a series of Au thicknesses ranging from 30 nm to 100 nm in order to optimize the SERS signals. Contrary to the evaporation method, the sputtering deposition adopted here ensures the 3D growth of the Au caps on top of the nanopillars, shrinking the inter-pillar separations as the Au deposition thickness increases. As the Au cap size grows, the gap size between them becomes smaller and sub-10 nm gaps are obtained when an Au thickness of 80 nm is deposited as shown in Figure 1d. It is also observed that a few gaps are closed and the Au caps start to touch each other, forming connecting Au islands (Figure 1c). The start of this touching effect is in fact beneficial to the field enhancement as will be discussed in the following. Nevertheless, beyond this critical thickness, though narrow gaps are also observed, more touching between the Au caps is present as shown in Figure S1 in the supporting information.

When metal nanostructures are placed in close adjacency, the plasmon resonances strongly interact and their overall response can be very different from that of the individual nanostructures.[26] The substrates we fabricated contain in fact a very high density of interacting Au nanocaps, where their global optical response is expected to smear out spectrally similar to aggregates of metal nanoparticles. Indeed, as shown in the reflection spectra measured with a Bruker Vertex 80v Fourier transform infrared spectrometer (**Figure 2**a, c), no sharp plasmonic resonances are observed for both nanopillar heights under investigation. In substrates with a thicker Au layer, nearly all the incident light is reflected in the near infrared. To gain more insight in the local optical response of the Au-capped Si nanopillar arrays, we have executed numerical FDTD simulations using Lumerical FDTD Solutions. Specifically, we implemented a FDTD model of Au nanospheroids standing on top of cylindrical Si nanopillars on a semi-infinite Si. The simulated reflection spectra are presented in Figure 2b, d, and they fit the experimental measurements well. Refer to Section 3 of the supporting information for more FDTD details.

Nanoscale RSCPublishing

COMMUNICATION

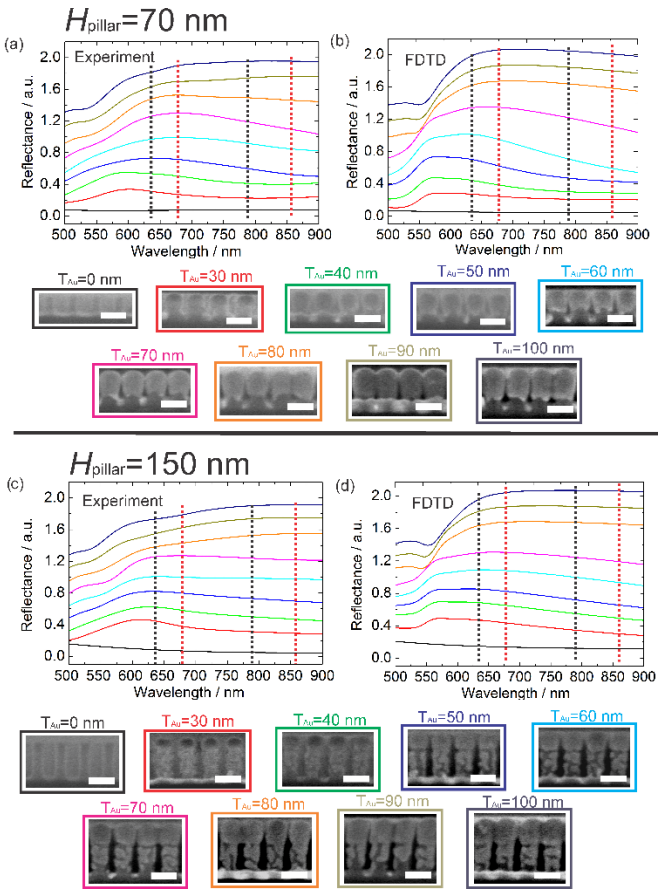

Figure 2. (a, c) Experimental and (b, d) FDTD simulated reflection spectra for the Au-capped nanopillar arrays with the nanopillar height of 70 nm and 150 nm. A series of Au thicknesses from 30 nm to 100 nm are deposited on the Si nanopillar arrays, and the corresponding cross section SEM images are exhibited at the bottom. The scale bars in the SEM images represent 100 nm. The spectra are off-set for clarity. The black dashed lines indicates the excitation wavelengths used in SERS measurements (633 nm and 785 nm), and the red ones are the corresponding stokes shifted wavelengths for the 4-ATP 1078 cm^{-1} vibrational mode (679 nm and 857 nm).

In spite of the fact that no sharp and pronounced plasmonic resonances are observed, this ultra-dense 'hot spot' array is promising for broadband SERS applications in the visible and near infrared range. Using 4-aminothiophenol (4-ATP) as a probe molecule, the SERS spectra for the H_{pillar}=70 nm and H_{pillar}=150 nm substrates were investigated at both 785 nm and 633 nm laser excitations, and the results are presented in **Figure 3**. Typically, the intensity of the C-S bond stretching vibrational mode at ~1078 cm^{-1}, which is highlighted in the green dashed box, increases from T_{Au}=30 nm to T_{Au}=80 nm Au depositions, as with the increasing Au thickness, the inter-pillar gaps narrow. For thicker Au layers, the intensity drops as a consequence of the touching Au caps. The T_{Au}=80 nm substrates, for which we have achieved the smallest gap size and lowest touching degree, show the maximum SERS intensities. Comparisons between the H_{pillar}=70 nm and H_{pillar}=150 nm substrates also indicate that the H_{pillar}=70 nm ones produce higher SERS signals.

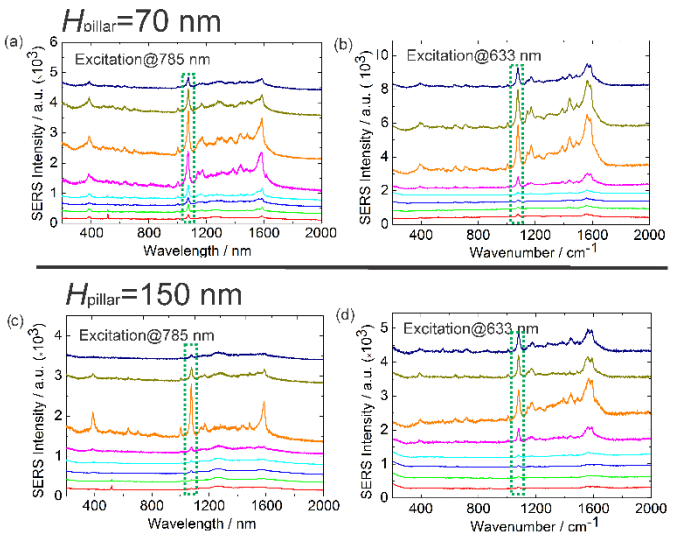

Figure 3. 4-ATP SERS spectra measured at (a, c) 785 nm and (b, d) 633 nm wavelength excitations for the Au-capped nanopillar arrays with the nanopillar height of 70 nm and 150 nm. The Au layer thicknesses range from 30 nm to 100 nm (same colour corresponding to the Au thickness as in Figure 2). The spectra are off-set for clarity. The green dashed box indicates the 4-ATP C-S bond stretching vibrational mode at ~1078 cm^{-1}.

The detected SERS signal is a complicated puzzle that deserves thorough scrutiny.[27,28] Typically it originates from EM and chemical enhancement mechanisms. The EM mechanism states that the enhancement factor (EF) equals the electric field intensity enhancement at the incidence wavelength multiplied by the enhancement at the stokes shifted wavelength, which could be approximated as the E^4 rule ($E^4=E^2_{incidence}\times E^2_{stokes}$). It is also established that the hot spots contribute more to the total SERS enhancement.[29,30] In our substrates, the maximum E^2 enhancement on the Au nanospheroid surface is also simulated as a function of the incidence wavelength (Supporting Information, Figure S2), which confirms that at the incidence and stokes wavelengths no pronounced resonances arise. This implies that the SERS signal mainly results from the non-resonant enhancement of the electric field intensity in the regions between the Au nanocaps. As displayed in Figure 1c, since both the nanogaps, where the Au caps do not touch, and the touching of the Au nanocaps are present in the array, the SERS enhancement is categorized into two effects as illustrated in **Figure 4**.

Nanoscale RSCPublishing

COMMUNICATION

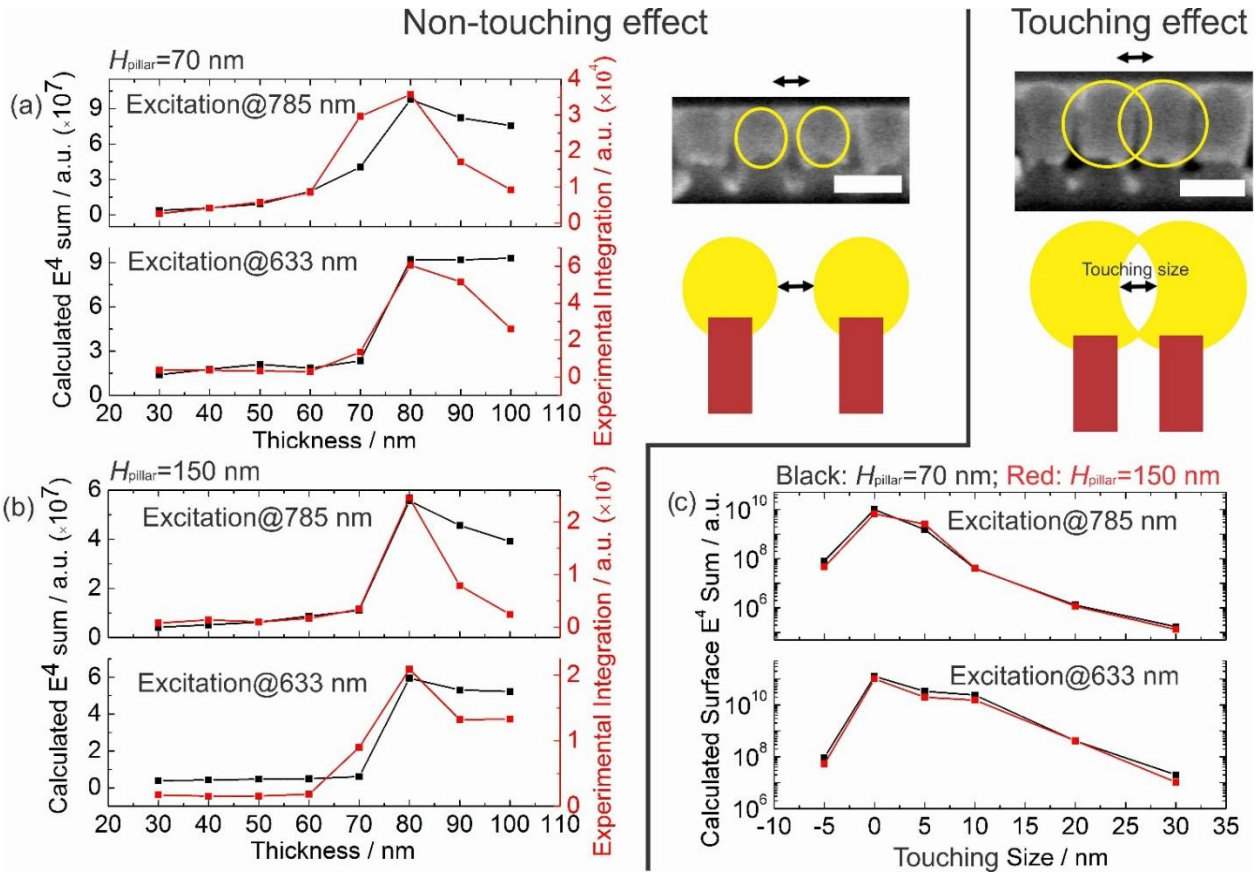

Figure 4. SERS signal enhancement interpretations based on FDTD simulations: (a, b) non-touching effect and (c) touching effect. For the Au caps that do not touch (e.g. prevalent in arrays with Au coating thicknesses of less than 70 nm, and also present in arrays with thicker Au coatings), the electric field intensity enhancement at the nanogap regions dominates. Here the non-touching effect applies. The calculated E^4 sum across the nanospheroid surface, the black curves corresponding to the left axes, and the experimental integrated SERS intensities, the red curves to the right axes, are demonstrated as a function of the Au deposition thickness for the nanopillar height of (a) 70 nm and (b) 150 nm, respectively. For arrays with thicker Au depositions, in addition to the non-touching effect, some of the Au caps start to touch and decrease the SERS intensity. (c) The calculated E^4 sum across the Au nanospheroid surface as a function of the touching size for the Au deposition thickness of 90 nm while keeping the vertical nanospheroid diameter as a constant. The touching size is defined as the diameter of the imaginary nanospheriod in the in-plane dimension minus the distance between adjacent nanospheroid centers as shown in the schematic of Figure 3c. Yellow spheroids in the SEM images approximate the outline of the Au caps.

For the thinner Au deposition thicknesses (T_{Au}<70 nm), the SERS signal enhancement is dominated by the high electric field enhancement located in the gap regions. Nanogaps are also observed in arrays with thicker Au coatings as shown in Figure S1. We call the field enhancement in these non-touching regions the *"non-touching"* effect. The enhancement factors due to the non-touching effect strongly depend on, not only the minimum distance between the gold surfaces of adjacent nanospheroids (gap size), but also other geometrical parameters such as the vertical nanospheroid diameter and the nanopillar height. While usually only the maximum field enhancement is considered in the EF calculation, here in order to take into account the overall topography of the electric intensity profile we will integrate the calculated the $E^2_{incidence} \times E^2_{stokes}$ product over the nanospheriod surface. As presented in Figure 4a, b, at both excitation wavelengths and for both nanopillar heights, this integrated field enhancement generally fits the trend of the experimental SERS signals. The spatially integrated field enhancement is a better fit to the experimental results in the sense that it considers the whole landscape of the electric field enhancement distribution across the nanospheroid surface instead of only the maximum E^4 enhancement at a specific position. In addition, the FDTD analysis shows that the surface E^4 sum for the H_{pillar}=70 nm substrates is larger than that for H_{pillar}=150 nm.

This could be attributed to the fact that the short nanopillars support a stronger constructive interference of the reflected light in the nanogap regions. Moreover, the higher Si nanopillars could absorb more light and effectively damp the plasmon, also reducing the SERS signals.

Moreover, it is noted that for the arrays with thicker Au depositions (T_{Au}≥90 nm), the experimental SERS signal intensity is smaller than the integrated E^4 enhancement predicted by the non-touching effect. This is because for these thicker Au coatings, in addition to the non-touching effect, the *"touching"* effect of the Au caps will eventually decrease the SERS signal. As more Au is deposited, a small fraction of the Au caps start to touch. Conceptually, at the beginning of the touching more enhanced hot spots will appear, resulting in further amplified signals (e.g. for arrays with gap sizes close to zero). As the deposition carries on, a larger faction of the Au caps are touching and more nanogaps start to diminish, impairing the SERS enhancement. As the FDTD simulation results demonstrate in Figure 4c, the calculated surface E^4 sum for the T_{Au}=90 nm substrates increases for a small touching size, and decreases when the touching size grows. This idea also corroborates the fact that it is the T_{Au}=80 nm arrays, in which clear touching just starts to show up, that presents the highest SERS signals. For these arrays with thicker Au coatings, the actual SERS signal enhancement could be considered as a combination of both the non-touching and touching effects. As thicker Au layer is deposited, the fraction of touching nanocaps is increasing, resulting in the reduced SERS signals. Therefore, fine-tuned Au deposition is critical to achieve optimized SERS signals.

In the H_{pillar}=150 nm substrates, it is clear from the SEM images in Figure 2 that on the Si nanopillar sidewalls there are Au nanoislands from the sputtering deposition. As previously reported,[14,15] these nanoislands could form gap-rich nanostructures that also contribute to the SERS signal enhancement. Nevertheless, in our highly dense arrays the SERS enhancement results from the gaps between the top Au caps instead. The simplified FDTD model without such sidewall nanoislands has already demonstrated an adequately good fit to the detected SERS intensities. In addition, the H_{pillar}=70 nm substrates, which lack the sidewall Au nanoislands, show an even higher SERS signal.

A limiting factor in the further widespread applications of the SERS technique is the trade-off between the high signal amplification and good uniformity. Nevertheless, since the major advantage of our Si nanopillar array is its high uniformity on a wafer scale, the Au capped substrates are expected to show a high SERS signal reproducibility. We compared our Au-capped nanopillar SERS substrates to the commercial Klarite™ from Renishaw Diagnostics. Among the best ever reported, Klarite™ SERS substrates are tested to show a relative signal standard deviation of better than 10%.[11,12] In addition, the geometry of the Klarite™ substrates, which are inverted Si pyramid arrays covered with Au, has been optimized for the coupling of localized and propagating surface plasmon modes to give resonances at 633 nm and 785 nm.[12] The Klarite™ hot spots are localized at the bottom and the top corners of the inverted pyramids with a pitch of ~2 μm. Since the uniformity of SERS signal largely depends on the experimental conditions, especially the laser spot size, it is recommended to use a >5 μm spot for the SERS excitation to ensure that adequate amount of inverted pyramids are illuminated. In our SERS measurement, a 10× water immersion objective with a laser spot of ~5 μm was used to fulfill the Klarite™ recommendation, and the SERS intensities are measured over a distance of 200 μm in a step of 1 μm. The mean intensity and standard deviation are calculated by integrating the 1078 cm^{-1} Raman band, and the coefficient of variation (CV) is defined as the standard deviation divided by the mean intensity, which is an indication of the SERS substrate uniformity. The comparison results between the Klarite™ and our nanopillar substrates (T_{Au}=80 nm) are shown in **Figure 5**. It demonstrates that the Au-capped nanopillar arrays not only present a higher SERS signal, but also a lower fluctuation/ CV level. On one hand, the improved signal reproducibility is related to the state-of-the-art nanofabrication process, which offers the high degree of inherent uniformity with an array pitch of less than 100 nm. On the other hand, it is attributed to the large number of hot spots that are easily accessible to the target analytes within the laser spot (~2.5×10^3 unit structures for our nanopillar substrates, compared to only ~5 for Klarite™, although the Au surface areas are similar). Compared to the literature with improved signal reproducibility,[9,10] our nanopillar substrates benefit from the large wafer level fabrication method. In addition, it features the sub-10 nm gap size which gives rise to the largely enhanced SERS signals.[16]

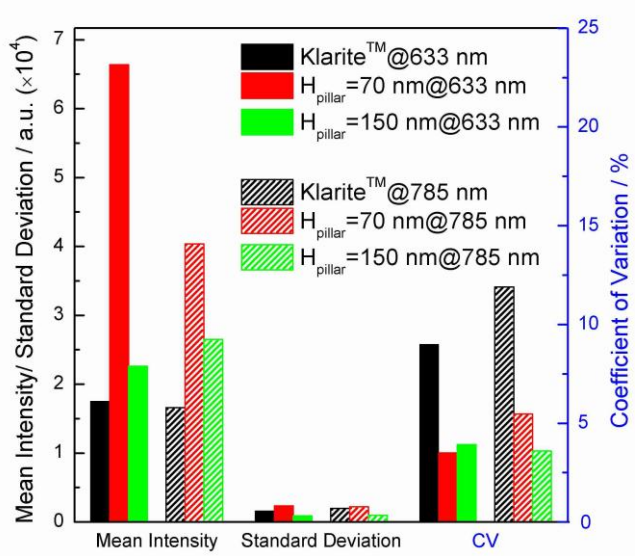

Figure 5. Uniformity comparisons of the T_{Au}=80 nm substrates with the commercial Klarite™. Compared to the Klarite™ substrate (CV~ 10%), the uniformity of the nanopillar supported substrates is much improved (CV~ 4%).

The substrate SERS EF of our Au capped nanopillar arrays have also been experimentally calculated as shown in Section 5 of the supporting information. It is noted that the EF calculation depends on the molecular coverage assumption adopted, and a variation as large as ~10^5 can be obtained.[19] Under the full monolayer coverage assumption, an average EF on the order of ~10^5 is attained in our calculation, while if few molecule coverage assumption is taken,[31] the EF can be ~10^9. In addition, since the nanogaps, the non-touching

regions of the Au caps, and the touching of the caps are both present in the T_{Au}=80 nm substrates, these experimental substrate EFs are the average values by taking into account both effects. The EF at particular Au cap positions with narrower gaps could be higher. In Table S2 in the supporting information, the simulated $E^4=E^2_{incidence}\times E^2_{stokes}$ at the maximum field enhancement positions on the surface for both *non-touching* and *touching* effects are also listed, which range from ~10^4 to ~10^8 depending on the gap sizes and excitation wavelengths. Therefore, the EF of our substrates could be sufficiently large for single molecule SERS detections, especially considering the high hot spot density and easy molecule accessibility.[32–35]

The goal of our current work is not to demonstrate an extremely large EF, but to present a scalable method to produce reliable SERS substrates with improved uniform and reproducible signals. The results in Figure 5 have shown that under the same experimental conditions, our nanopillar substrates surpass the commercial Klarite™ substrates with an improved SERS performance. Batch-to-batch reproducibility of our SERS substrates has also been investigated, and they demonstrates good reliability as well (Section 6 in the supporting information).

Conclusions

In conclusion, we have introduced a method to realize large wafer scale preparation of exceptionally dense arrays of plasmonic hot spots with sub-10 nm gaps, and we demonstrate that these substrates support both high SERS enhancement factors and excellent uniformity and reproducibility. Specifically, employing the state-of-the-art CMOS front-end patterning techniques allowed us to develop a 300 mm wafer scale process for the fabrication of ultra-dense arrays of Si nanopillars, which we subsequently coated with Au films to obtain a pattern of Au nanocaps with sub-10 nm gaps. We have investigated the SERS performance of substrates under both 785 nm and 633 nm excitations. Largely enhanced and uniform SERS signals have been obtained in the ultra-dense arrays and compared to the commercial Klarite™ substrates. Though no pronounced plasmonic resonances are detected, FDTD simulations illustrate that the amplified SERS signals are mainly derived from the electric field enhancement in the regions between the Au caps. Due to the large signal enhancement, high uniformity and wafer scale fabrication capacity, the Au-capped nanopillar substrates are promising for the detection of small molecules in label-free biosensing applications.

Acknowledgements

C.C. and N.V. gratefully acknowledge the financial support from FWO (Flanders). N.V. and V.V.M. are supported by the Methusalem funding by the Flemish Government.

Notes and references

[a] IMEC, Kapeldreef 75, B-3001 Leuven, Belgium. E-mail: lijackie@imec.be, chang.chen@imec.be

[b] INPAC and Department of Physics and Astrnomy, KU Leuven, Celestijnenlaan 200 D, B-3001 Leuven, Belgium.

[c] Panasonic Corporation, 3-4 Hikaridai, Seika-cho, Soraku-gun, Kyoto 619-0237, Japan.

Electronic Supplementary Information (ESI) available: [SEM images of nanopillar substrates, FDTD simulation details, electric field enhancement maximum on Au nanospheroid surface, substrate SERS enhancement factor calculation, batch-to-batch reproducibility]. See DOI: 10.1039/c000000x/

1. A. Polemi, S. M. Wells, N. V. Lavrik, M. J. Sepaniak, and K. L. Shuford, *J. Phys. Chem. C*, 2011, **115**, 13624–13629.
2. J. D. Caldwell, O. Glembocki, F. J. Bezares, N. D. Bassim, R. W. Rendell, M. Feygelson, M. Ukaegbu, R. Kasica, L. Shirey, C. Hosten, and C. E. T. Al, *ACS*, 2011, **5**, 4046–4055.
3. G. H. Gu, J. Kim, L. Kim, and J. S. Suh, *J. Phys. Chem. C*, 2007, **111**, 7906–7909.
4. C. Chen, J. A. Hutchison, P. Van Dorpe, R. Kox, I. De Vlaminck, H. Uji-I, J. Hofkens, L. Lagae, G. Maes, and G. Borghs, *Small*, 2009, **5**, 2876–82.
5. Z. Huang, G. Meng, Q. Huang, Y. Yang, C. Zhu, and C. Tang, *Adv. Mater.*, 2010, **22**, 4136–9.
6. D.-K. Lim, K.-S. Jeon, H. M. Kim, J.-M. Nam, and Y. D. Suh, *Nat. Mater.*, 2010, **9**, 60–7.
7. L. a. Dick, A. D. McFarland, C. L. Haynes, and R. P. Van Duyne, *J. Phys. Chem. B*, 2002, **106**, 853–860.
8. S. Gómez-Graña, J. Pérez-Juste, R. a. Alvarez-Puebla, A. Guerrero-Martínez, and L. M. Liz-Marzán, *Adv. Opt. Mater.*, 2013, **1**, 477–481.
9. W. J. Cho, Y. Kim, and J. K. Kim, *ACS Nano*, 2012, **6**, 249–55.
10. N. G. Greeneltch, M. G. Blaber, A.-I. Henry, G. C. Schatz, and R. P. Van Duyne, *Anal. Chem.*, 2013, **85**, 2297–303.
11. M. E. Hankus, D. N. Stratis-cullum, and P. M. Pellegrino, in *SPIE-Optics and Photonics West*, 2011, vol. 8099, pp. 8099–7.
12. N. M. B. Perney, J. J. Baumberg, M. E. Zoorob, M. D. B. Charlton, S. Mahnkopf, and C. M. Netti, *Opt. Express*, 2006, **14**, 847–57.
13. K. Malachowski, R. Verbeeck, T. Dupont, C. Chen, Y. Li, S. Musa, T. Stakenborg, D. Sabuncuoglu Tezcan, and P. Van Dorpe, *ECS Trans.*, 2013, **50**, 413–422.
14. W. Li, F. Ding, J. Hu, and S. Y. Chou, *Opt. Express*, 2011, **19**, 3925–36.
15. Y.-J. Oh and K.-H. Jeong, *Adv. Mater.*, 2012, **24**, 2234–7.
16. U. S. Dinish, F. C. Yaw, A. Agarwal, and M. Olivo, *Biosens. Bioelectron.*, 2011, **26**, 1987–92.
17. J. D. Caldwell, O. J. Glembocki, F. J. Bezares, M. I. Kariniemi, J. T. Niinistö, T. T. Hatanpää, R. W. Rendell, M. Ukaegbu, M. K. Ritala, S. M. Prokes, C. M. Hosten, M. a Leskelä, and R. Kasica, *Opt. Express*, 2011, **19**, 26056–64.
18. A. Shevchenko, V. Ovchinnikov, and A. Shevchenko, *Appl. Phys. Lett.*, 2012, **100**, 171913.
19. M. S. Schmidt, J. Hübner, and A. Boisen, *Adv. Mater.*, 2012, **24**, OP11–18.
20. X. Yang, H. Zhong, Y. Zhu, J. Shen, and C. Li, *Dalt. Trans.*, 2013, **42**, 14324–30.
21. R. Lu, J. Sha, W. Xia, Y. Fang, L. Gu, and Y. Wang, *CrystEngComm*, 2013, **15**, 6207.
22. F. Ou, M. Hu, I. Naumov, and A. Kim, *Nano Lett.*, 2011, **11**, 2538–2542.

23. M. A. Rafiq, H. Mizuta, S. Uno, and Z. A. K. Durrani, *Microelectron. Eng.*, 2007, **84**, 1515–1518.
24. H. C. Jeon, C.-J. Heo, S. Y. Lee, and S.-M. Yang, *Adv. Funct. Mater.*, 2012, **22**, 4268–4274.
25. X. Yang, N. Ileri, C. C. Larson, T. C. Carlson, J.A. Britten, A.S.P. Chang, C. Gu, and T.C. Bond, *Opt. Express*, 2012, 20, 24819–24826.
26. P. K. Jain, W. Huang, and M. a. El-Sayed, *Nano Lett.*, 2007, **7**, 2080–2088.
27. S. M. Morton, D. W. Silverstein, and L. Jensen, *Chem. Rev.*, 2011, **111**, 3962–94.
28. E. C. Le Ru, M. Meyer, and P. G. Etchegoin, *J. Phys. Chem. B*, 2006, **110**, 1944–8.
29. C. Chen, J. A. Hutchison, F. Clemente, R. Kox, H. Uji-I, J. Hofkens, L. Lagae, G. Maes, G. Borghs, and P. Van Dorpe, *Angew. Chemie*, 2009, **48**, 9932–5.
30. Y. Fang, N.-H. Seong, and D. D. Dlott, *Science (80-.).*, 2008, **321**, 388–392.
31. M. Hu, F. S. Ou, W. Wu, I. Naumov, X. Li, A. M. Bratkovsky, R. S. Williams, and Z. Li, *J. Am. Chem. Soc.*, 2010, **132**, 12820–2.
32. E. C. Le Ru, E. Blackie, M. Meyer, and P. G. Etchegoin, *J. Phys. Chem. C*, 2007, **111**, 13794–13803.
33. P. G. Etchegoin and E. C. Le Ru, *Phys. Chem. Chem. Phys.*, 2008, **10**, 6079–89.
34. J. P. Camden, J. a Dieringer, Y. Wang, D. J. Masiello, L. D. Marks, G. C. Schatz, and R. P. Van Duyne, *J. Am. Chem. Soc.*, 2008, **130**, 12616–7.
35. D. Wang, W. Zhu, M. D. Best, J. P. Camden, and K. B. Crozier, *Sci. Rep.*, 2013, **3**, 2867.